Journal Pre-proofs

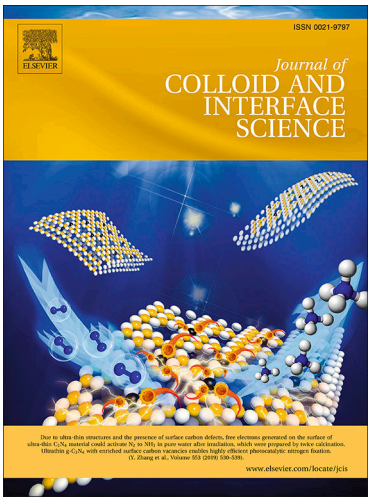

Curved membrane structures induced by native lipids in giant vesicles

Karthika S Nair, Neethu B Raj, K Madhavan Nampoothiri, Gayathri Mohanan, Silvia Acosta-Gutiérrez, Harsha Bajaj

PII: S0021-9797(21)02235-9
DOI: https://doi.org/10.1016/j.jcis.2021.12.098
Reference: YJCIS 29437

To appear in: *Journal of Colloid and Interface Science*

Received Date: 23 November 2021
Revised Date: 14 December 2021
Accepted Date: 15 December 2021

Please cite this article as: K.S. Nair, N.B. Raj, K. Madhavan Nampoothiri, G. Mohanan, S. Acosta-Gutiérrez, H. Bajaj, Curved membrane structures induced by native lipids in giant vesicles, *Journal of Colloid and Interface Science* (2021), doi: https://doi.org/10.1016/j.jcis.2021.12.098

Curved membrane structures induced by native lipids in giant vesicles

Karthika S Nair[a], Neethu B Raj[a], K Madhavan Nampoothiri[a,b], Gayathri Mohanan[a], Silvia Acosta-Gutiérrez[c,], Harsha Bajaj[a,b,]**

[a]Microbial Processes and Technology Division,
CSIR- National Institute for Interdisciplinary Science and Technology (NIIST),
Trivandrum 695019, Kerala, India

[b]Academy of Scientific and Innovative Research (AcSIR),
CSIR-Human Resource Development Centre,
Ghaziabad 201002, India

[c]Department of Chemistry,
Institute of Structural and Molecular Biology,
University College London, UK

*Corresponding author e-mail: harshabajaj@niist.res.in;
s.gutierrez@ucl.ac.uk

Keywords: Giant vesicles, Native lipids, Lipopolysaccharides, Membrane deformation, Curved membrane, Spontaneous curvature, Bending Rigidity.

Abstract: Native lipids in cell-membrane support crucial functions like intercell communication via their ability to deform into curved membrane structures. Cell membrane mimicking Giant unilamellar vesicles (GUV) is imperative in understanding native lipid's role in membrane transformation however remains challenging to assemble. We construct two giant vesicle models mimicking bacterial inner-membrane (IM) and outer-membrane (OM) under physiological conditions using single-step gel-assisted lipid swelling. IM vesicles composed of native bacterial lipids undergo small-scale membrane remodeling into bud and short-nanotube structures. In contrast, OM vesicles asymmetrically assembled from Lipopolysaccharide (LPS) and bacterial lipids underwent global membrane deformation under controlled osmotic stress. Remarkably, highly-curved structures mimicking cell-membrane architectures, including daughter vesicle networks interconnected by necks and nano-tubes ranging from micro to

nanoscale, are generated in OM vesicles at osmotic stress comparable to that applied in IM vesicles. Further, we provide a quantitative description of the membrane structures by experimentally determining membrane elastic parameters, i.e., neck curvature and bending rigidity. We can conclude that a larger spontaneous curvature estimated from the neck curvature and softer membranes in OM vesicles is responsible for large-scale deformation compared to IM vesicles. Our findings will help comprehend the shape dynamics of complex native bacterial lipid membranes.

1. Introduction

Cell membrane plays a central role in cell functions, ranging from physical barriers to deformation for controlled signaling over molecular events. One hallmark property of cell membranes is their ability to change shape via physical perturbation of lipid membranes supported by curvature generating proteins for crucial cell functions, including division [1,2]. Other essential functions of cells like intercellular communication, endocytosis, or pathogenesis are assisted by curved membrane structures in the form of nano-tubes and pearl-like chains [3,4]. Such diverse roles of membranes are sustained by a considerable extent of the lipid's structural and chemical diversity in cells [5].

Giant unilamellar vesicles (GUV's) have been the model of choice to control and mimic such cellular membrane shapes for bottom-up biology applications, including understanding the localization properties of proteins [6]. Previous studies on curvature-protein-induced deformation in synthetic cells have been predominantly reported in lipid mixtures that remotely mimic cellular membranes [7–9]. Local spontaneous curvature is also generated by an asymmetry of ions and macromolecules apart from proteins across membranes, inducing shape changes, which have been described mainly in simple lipid vesicles [10–13]. Although, complex native lipids like glycolipids are suggested to remodel membranes by affecting their intrinsic curvature and modifying the membrane bending rigidity [14–16]. Meticulous membrane transformation studies triggered by complex lipids are restricted to ganglioside (GM1), rhamnolipid-induced deformation, and glycocalyx [10,17–20]. Previously, lipopolysaccharide (LPS)-induced transformations were reported in vesicles composed of lipids distantly mimicking physiological compositions and buffer conditions [21,22]. Notably, the morphologies in these reports [22] were observed even in the absence of LPS merely due to osmotic deflation. Moreover, spontaneous absorption of LPS into and out of lipid membrane of

vesicles with no control over the process suggests an ambiguous role of LPS in the morphologies observed previously [21,22]. Likewise, technical challenges and complex strategies in the stable reconstitution of lipids like full-length LPS in vesicles have limited the quantitative understanding of LPS induced deformations in cell-mimicking membranes [14,23,24].

We engineer giant liposome assemblies, including IM and OM (LPS) vesicles mimicking both inner-membrane and outer-membrane using simple single-step lipid hydration. The vesicle systems offer a stable platform to investigate unambiguously surface membrane deformations triggered by native bacterial lipids. Finally, we provide quantitative membrane mechanical parameters to elucidate the membrane deformation in both vesicle systems.

2. Experimental Methods

2.1 . Materials

Escherichia coli polar lipid extract, 1,2-dipalmitoyl-sn-glycero-3-phosphocholine (DPPC, 99%) (both from Avanti Polar Lipids, Inc.), Mowiol 28-99 (MW 145,000 Da) fully hydrolyzed Polyvinyl alcohol (PVA, 98%), fluorescein isothiocyanate isomer I (FITC) labelled Lipopolysaccharide from *E. coli* O55:B5, Lipopolysaccharide (LPS) from *E. coli* O55:B5, ATTO-488 1,2-Dioleoyl-sn-glycero-3-phosphoethanolamine(DOPE, > 90%), ATTO-550 DOPE (>80%), Bovine serum albumin (BSA, >98%), Potassium hydroxide (KOH, >95%), Sodium chloride (NaCl, 98%), Potassium chloride (KCl, 98%), 4-(2-hydroxyethyl)-1-piperazineethanesulfonic acid (HEPES, 99.5%), Calcium Chloride ($CaCl_2$, >98%), Sucrose (>99.5%), Sodium dodecyl sulphate (SDS, >99%), Trypan Blue, Acridine Orange 10-nonyl bromide (>90%) and other chemicals used in this study are from Merck (Sigma-Aldrich) unless mentioned otherwise. Alexa-Fluor 488 Lipopolysaccharide from *E. coli* O55:B5 is from Thermo Fischer Scientific. Vacuum grease is from Dow corning. Glass slides (26x 76mm, 1mm thickness, lab tech), Coverslips (22mm x 0.13mm thickness) are from Blue star, reagent barriers (20mm diameter x 1mm depth) from Grace Biolabs, and Syringes from Hamilton.

2.2. Vesicle preparation

Vesicles are prepared using the Gel-assisted swelling method [25]. Poly-vinyl alcohol or PVA (5% w/v) coated slides for the gel-assisted formation of GUVs are prepared using previously described methods [26]. The lipid film is coated on the PVA slides and subsequently hydrated by adding salt buffer (200 µl of 137 mM NaCl, 2.7 mM KCl, 2 mM $CaCl_2$ in10 mM HEPES pH

7) inside an O-ring to form vesicles. The same buffer is used throughout the study. The vesicle solution is then pipetted using a cut tip.

Inner-membrane (IM) mimicking vesicles: *Escherichia coli* polar lipid extract (1.5 mg/ml, 20 µl referred to as Inner-membrane or IM lipid extract; Figure S1) dissolved in chloroform is spread on the PVA film and kept in a desiccator. ATTO-488 DOPE (0.5 mol%) or ATTO-550 DOPE (0.05 mol%) is added along with lipid solution for membrane morphology experiments. The salt buffer is added to the lipid film and incubated in a water bath at 40° C for 10 minutes.

Outer-membrane (OM) mimicking vesicles: Briefly, lipopolysaccharide (LPS) vesicles mimicking the outer-membrane composition are formed by inverse-phase precursor film coating using gel-assisted technology (details in SI text 1.1). The aqueous lipopolysaccharide solution is vigorously blended with *E. coli* Polar lipid solubilized in chloroform to form an opalescent mixture of inverted LPS-lipid micelle (Figure 1) coated on PVA film. LPS is mixed with *E. coli* lipid extract at different molar ratios of LPS: IM lipids. Salt buffer is added inside the O-ring and incubated in a water bath at 42° C for 20 minutes. Fluorescently labeled LPS (FITC-LPS or Alexa-Fluor 488 LPS) are utilized to detect LPS reconstitution. Effective LPS: IM lipid ratio is estimated by normalizing fluorescence intensity of vesicles prepared from different LPS: IM ratios (SI text 1.1 and Table S1) as described previously [27]. We utilize vesicles with initial molar ratios of 1:6 or 8:48 (LPS: IM) at a final concentration of 100 µM of LPS and 600 µM of IM lipids (assuming the LPS molecular weight to be 20 kDa) for subsequent studies. All the measurements are done by diluting the sample 5-10 times to minimize the fluorescence from free LPS in the external buffer. Cardiolipin in vesicles is detected using acridine orange 10-nonyl bromide (SI text 1.1.1). Cardiolipin reconstitution is similar in both IM and OM vesicles based on fluorescence intensity (Figure S2).

2.3. Asymmetric reconstitution of glycolipid- Quenching assay

A fluorescence quenching assay using trypan blue is employed to investigate any asymmetry in the reconstitution of LPS in OM vesicles. The addition of quencher like trypan blue to fluorescently labeled vesicles quenches the fluorescence of the lipids in the outer-leaflet due to its inability to cross the lipid barrier, based on which lipid symmetry is concluded [28,29]. Trypan blue (TB 500 µM) is added to the vesicle sample in the imaging chamber, followed by 5-minute incubation and imaging. Next, sodium dodecyl sulfate (SDS, 500 µM) is added to the same vesicle to gently rupture the membrane and incubated with TB for 5 minutes, followed by

imaging. The fluorescence intensity of the rim of LPS vesicles is analyzed before and after treatment with TB and SDS. First, the rim intensity is determined using Fiji, points are made on the rim of the vesicle, and the fluorescence intensity is averaged over at least 10 points on the rim (I_{rim}). Next, the fluorescence intensity outside the vesicle is calculated (I_{out}). The field outside of the vesicles is set to zero by subtracting the background intensity for attaining the final rim intensities $I_f = (I_{rim} - I_{out})$. The final fluorescence intensity after background subtraction is calculated before (I_{fb}) and after the treatment (I_{fa}) with trypan blue and detergent SDS (I_{fad}). The intensity before TB treatment is normalized to 1 for each vesicle, and intensity after TB (I_{fa}) and detergent treatment (I_{fad}) is normalized relative to I_{fb} to estimate the asymmetry in LPS reconstitution based on fluorescence.

2.4. Membrane deformation in vesicles

Chambers are prepared on the passivated glass slides using reagent barriers (details in SI text 1.2 Passivation of slides). One corner of the in-house chamber made of barrier (Figure S3) is cut to provide a path through which external hypertonic solution is added using a syringe. The vesicle volume or membrane tension is controlled by step-wise osmotic pressure by exposing vesicles to the hypertonic sucrose solution (prepared in salt buffer), removing water from vesicles to dilute the external sucrose creating an increased membrane area to volume ratio. For membrane morphology experiments, 0.5 mol% of ATTO-488 DOPE or 0.05 mol% of ATTO-550 DOPE is added along with lipid solution for better visualization in fluorescence. Both FITC (at 1:6 FITC-LPS: IM) and Alexa-Fluor 488 labeled LPS vesicles (0.25 mol% with unlabelled LPS: IM at initial 1:6 or 8:48 ratio) are utilized to check the effect of fluorescent dyes on vesicle morphologies.

Briefly, LPS(OM) or IM GUV samples are added into the chamber, and a coverslip is placed on top. The vesicles are allowed to settle down for 2-4 minutes. The salt buffer contains 137 mM NaCl, 2.7 mM KCl, 2 mM $CaCl_2$ in10 mM HEPES pH 7, and the sucrose stock solution of 500 mM or 750mM sucrose is made in the same salt buffer to generate osmotic stress. Step-wise, adding hypertonic sucrose solution for LPS vesicles (5 µl of 500 mM sucrose in salt buffer) or IM vesicles (5µl of 750 mM sucrose in salt buffer) is done through the cut path using a Hamilton-syringe every 5 minutes. The applied osmotic pressure is described by the ratio $r = P_f/P_i$ where, P_f is the final osmolarity and P_i is the initial osmolarity of the solution outside GUVs in the slide chamber. Two sets of experiments are performed after step-wise addition of hypertonic sucrose solutions to vesicles. Initially, vesicles are imaged at $r = 1$ to understand

the batch's quality, a minimum of n = 15-30 vesicles are imaged, and any defects on the vesicle surface are recorded before applying osmotic pressure. Time-resolved measurements are conducted to understand the physical membrane remodeling in individual vesicles. A hypertonic solution is added till we start observing shape change, and the final osmolarity ratio is made from $1.3 \leq r \leq 1.8$ for OM vesicles and $1.6 \leq r \leq 1.9$ for IM vesicles. In the second round of the experiment, a scan is performed on the same slide to obtain a statistical analysis of the various morphologies observed at corresponding r values.

To note, a higher osmolarity ratio is required for IM vesicles compared to LPS vesicles to induce any transformation. Both ATTO-488 and ATTO-550 labeled vesicles show similar morphologies in OM and IM vesicles. The images/movies are recorded after 5 minutes of every sucrose addition or corresponding r value. More details related to additional control experiments are presented in SI text 1.3.

2.5. Theoretical analysis of morphologies

The membranes in both IM and OM vesicles have a uniform composition at room temperature. Hence, their shape can be primarily defined by the uniform elastic properties of bending rigidity (k) and the spontaneous curvature (m). Membrane shape can then be governed by bending energy[30] defined by

$$E_{be} = \int \mathrm{dA2k\,(M - m)^2} \qquad [1]$$

Under the current experimental conditions where the temperature remains constant, and the vesicle volume is controlled by osmotic pressure, we assume that the vesicle's membrane area (A) remains constant [31] as estimated in SI section 1.4. The bending energy will vanish if the mean curvature (M) equals the spontaneous curvature (m).

2.5.1. Spontaneous curvature

Spontaneous curvature (m) can be generated by various molecular processes of asymmetric adsorption of ions, small molecules, lipids, or proteins on vesicle membranes [32]. Here, we applied hypertonic sucrose solutions outside vesicles to deflate them. The vesicles prepared in salt buffer (137 mM NaCl, 2.7 mM KCl, 2 mM $CaCl_2$ in10 mM HEPES pH 7) are exposed to sucrose solutions made in the same salt buffer. Hence the vesicles are now exposed internally to salt, and the external leaflet is exposed to sucrose (and salt), creating an asymmetry of sugar solution. We propose to generate a slight spontaneous curvature due to the adsorption of asymmetric sucrose solutions on vesicle outer-leaflet. As the membrane bends away from the external membrane leaflet, the morphologies observed in IM and OM vesicles, we assign a

positive spontaneous curvature for the morphologies.

Hence, we estimate the spontaneous curvature from the geometry of the morphologies. In IM vesicles, the primary morphology observed at the highest applied osmotic pressure ($r = 1.9$) is vesicle budding. For homogenous membranes like in IM vesicles, the spontaneous curvature given by equation [2] can be determined by the neck condition connecting the mother vesicle and bud. Hence the neck curvature (M_n) determines the lower bound of spontaneous curvature of individual morphology.

$$m \geq M_n = \frac{1}{2}\left(\frac{1}{R_{mother}} + \frac{1}{R_{bud}}\right) \qquad [2]$$

The two significant morphologies in OM vesicles include multi-daughter vesicles with or without nano-tubes connected by membrane necks at the highest osmotic pressure applied. As the OM vesicle membrane is optically homogenous at room temperature, the spontaneous curvature is determined by imposing the neck condition. If the neck curvature ~~(M_n)~~ is larger than the spontaneous curvature of the vesicle, the closed neck is unstable and opens up. Hence a boundary condition can be imposed to obtain quantitative membrane elastic parameter of spontaneous curvature (m). The following condition needs to be satisfied $m \geq M_n$, to prevent the necks from opening. The multi-daughter morphologies will not be stable if each of the necks connecting adjacent daughter vesicles opens up, giving rise to the neck conditions where,

$$m \geq M_n = \frac{1}{2}\left(\frac{1}{R_1} + \frac{1}{R_2}\right) \qquad [3]$$

Here we calculate the neck curvature by measuring the radius of the smallest connecting daughter vesicles (R_1 and R_2) or determining the largest neck curvature, which will estimate the lower bound of the spontaneous curvature. The diameters of individual daughter or mother vesicles are calculated by measuring the intensity profile across the vesicle rim. A line plot is drawn across the vesicle's diameter to obtain a fluorescence intensity profile (Figure 1). The x-axis values corresponding to intensity peaks in the plot profile are subtracted to get the diameter of a vesicle. All the analysis and Figures are done using ImageJ/Fiji (https://imagej.net/Fiji). For the budding and multi-vesicle morphologies connected by membrane necks as described in (Figure 2, Figure 3, and Figure 4), a mean neck curvature [31,33,34] can be defined as equation [3]. For such a morphology to be stable, all the membrane necks connected to the individual vesicles must be stable. The highest neck curvature of an individual morphology provides the best estimate of spontaneous curvature (lower bound). We experimentally determine the neck curvature using eq. 3 to estimate the spontaneous curvature (m) based on the geometry of

specific morphology. An average of at least 50 independent neck curvatures is determined to obtain the vesicle membrane's average spontaneous curvature (lower bound).

Multi-daughter with nano-tube structures also form a large part of the population, where the spontaneous curvature of membranes forming nano-tube can be deduced from the radius of the cylindrical tubes [6] defined by

$$m = 1/2R_{cyl} \qquad [4]$$

We estimate the spontaneous curvature of the Multi-daughter with nano-tube morphology in OM vesicles by calculating the diameter of the nano-tubes from the estimated constant area of the vesicle as described in SI section 1.4. The estimated tube diameters (from at least 3 independent structures) range from 100 nm to 300 nm, and the spontaneous curvature is calculated from eq. 4.

2.5.2. *Bending rigidity measurements*

The bending rigidity is calculated from the fluctuation spectrum of vesicles [35,36]. The IM and OM vesicles doped with a few mol% of fluorescently labeled lipid are exposed to hypertonic sucrose until they start fluctuating, and videos are recorded in epifluorescence mode. In order to retrieve the fluctuation spectrum from the videos of the undulating vesicles, we first corrected the drift motion of the vesicles in Fiji using the StackReg plugin(https://imagej.net/Fiji). We extracted the spectrum of the vesicle contour fluctuations about the mean radius using the previously described method [36] with the MATLAB scripts provided (MATLAB, R2021a. Natick, Massachusetts: The MathWorks Inc.). The obtained fluctuating amplitudes are independent and have a mean square amplitude dependent on the membrane bending rigidity κ and the tension σ,

$$< \overrightarrow{\mu_q}(t)\overrightarrow{\mu_q^*}(t) >= \frac{k_B T}{\kappa(q^4 + \bar{\sigma}q^2)}, \qquad [5]$$

where $k_B T$ is the thermal energy and $\bar{\sigma} = \sigma R^2/\kappa - 2H_0 R + 2H_0^2 R^2$ where H_0 is the mean curvature, and R is the radius.

We fitted equation 5 using the least-squares method implemented in the python library Scipy [37] for all the videos analyzed in this work. The bending rigidity parameter is very sensitive to the optical mode range used to fit the variance of the spectrum amplitude, and it varies for every video. In each case, we selected the range that minimizes the residuals, fitting parameters, and q ranges are provided in TableS2 for each video. The previously described spontaneous curvature of the imaged vesicles poses an extra challenge to fit both the contour fluctuations and the obtained variance of the spectrum amplitude. It must be considered in calculating the membrane tension, σ, from the fitted spectrum.

2.6. Optical Set-up

All images or videos are taken in Olympus IX83 Inverted Microscope, Carl Zeiss Axio imager2 upright microscope with epifluorescence module, and N-SIM A1R Nikon confocal microscope. A 4.2MP Photometrics Prime BSI sCMOS with 13.3 mm x 13.3 mm,18.8 mm diagonal Sensor area is used in Olympus microscope. The Carl Zeiss microscope employs a 2.83 MP Axiocam 503 monochrome with 1936 (H) × 1460 (V) sensor pixel count. A 40x (NA 0.75) objective is used to image the phenomenon of the LPS and IM vesicles membrane morphology. Both phase contrast and fluorescence images of LPS incorporation and different membrane morphology phenomenon are snapped using a 60X (NA 1.42) and 100X (NA 1.45) oil objective.

3. Results and Discussion

3.1. Assembly of native lipids into giant vesicles

We assemble native bacterial lipids into giant vesicles mimicking both inner-membrane (IM) and outer-membrane (OM) (**Figure 1**A and 1B). IM vesicles are prepared using Gel-assisted hydration with native bacterial IM lipids. For stable LPS reconstitution in OM vesicles with IM lipids, we employ inverse-phase precursor film assembly on the hydrogel-assisted swelling technique as described in Methods (Figure 1C). LPS integration in the membrane is confirmed by incorporating fluorescently labeled LPS like FITC or Alexa-Fluor 488. The fluorescence intensity peaks depict successful assembly at the vesicle rim irrespective of the label employed (Figure 1D, Figure S4). Notably, IM vesicles lack the fluorescence intensity peaks at the membrane rim without fluorescent-labeled lipids (Figure S5 A1 and A2). OM and IM vesicles are formed under physiological salt conditions (137mM NaCl, 2.7 mM KCl and 2mM $CaCl_2$ pH 7). In addition, an average diameter of 15 ± 5 μm is obtained for LPS reconstituted vesicles (Figure S5 B, N= 6 batches, n=380 vesicles).

To investigate the effective or actual fraction of LPS in the OM vesicles, we incorporate LPS: IM at different ratios (Figure S5 C). LPS lipids used contained a small (1:9) fraction of fluorescently labeled LPS. After vesicle formation, the mean fluorescence of the liposomes is expected to scale according to the amount of fluorescently labeled LPS if the initial and actual concentrations are maintained. We observed that the actual effective reconstitution of LPS is maintained till specific ratios (2: 48 or 25:600) and above which the normalized intensity increases but does not scale corresponding to the expected fluorescence intensity (Figure 1E). For an initial mol ratio of 8: 48, the effective ratio based on normalized fluorescence intensity

(4.9± 1.9) is estimated to be 4.9± 1.9: 48 LPS: IM (Figure 1E). The large standard deviations in normalized intensity represent vesicle to vesicle variations (N=2 batches, n= 60 vesicles from each set of LPS concentration). For further experiments, vesicles are prepared with an initial LPS: IM lipid at 8:48 or 100:600 molar ratio and effective mol ratio of 61 ± 24: 600 to resemble bacterial outer-membrane composition (1:9) [38].

Additionally, we investigate the possibility of asymmetric reconstitution of LPS in the vesicle system with fluorescently labeled LPS using trypan blue quenching assay. The normalized intensities before (I_{fb}) and after treatment (I_{fa}) with TB are presented for single vesicles (Figure S6). A mean value of I_{fa} = 0.41± 0.16 is reported for normalized intensity after addition of TB (N = 3 , n = 49 vesicles). We confirm a mild asymmetry in glycolipid reconstitution in vesicles with outer-leaflet enriched in glycolipid due to the quenching of total vesicle-rim fluorescence by 60%. The results are further validated where almost full quenching is observed after detergent addition suggesting diffusion of TB to vesicle lumen and quenching the lipids in the inner-leaflet of vesicles (Figure S7).

Further, the stability of LPS reconstitution is determined in our system based on the fluorescence intensity of LPS-labeled individual vesicles. The normalized intensity is observed immediately after preparation and 24 hours of sample incubation at 4°C. Negligible changes in relative intensity of Alexa labeled LPS vesicles are reported, confirming no absorption or desorption of LPS into or from outer-leaflet of vesicle membranes for 24 hours (N=2 independent batches, n=95 individual vesicles) (Figure S8). We can affirm stable reconstitution and no absorption or desorption of LPS into or out of the OM vesicles in contrast to previous studies [19,21,22].

A complex-two-step procedure was devised earlier to reconstitute LPS in native lipid vesicles using the electroformation method which may lead to lipids oxidation [23]. Another work [24] assembled full-length LPS asymmetrically in vesicles using water-in-oil emulsion; however, the assembly was feasible only for specific inner-leaflet lipid compositions that remotely mimicked bacterial lipid composition. Here we introduce a much simpler one-step hydration procedure for constructing LPS-vesicles without the risk of any lipid modification under physiological mimicking conditions. We specifically establish the efficient, controlled, and stable assembly of native and complex lipids like LPS into vesicles to conduct deformation studies.

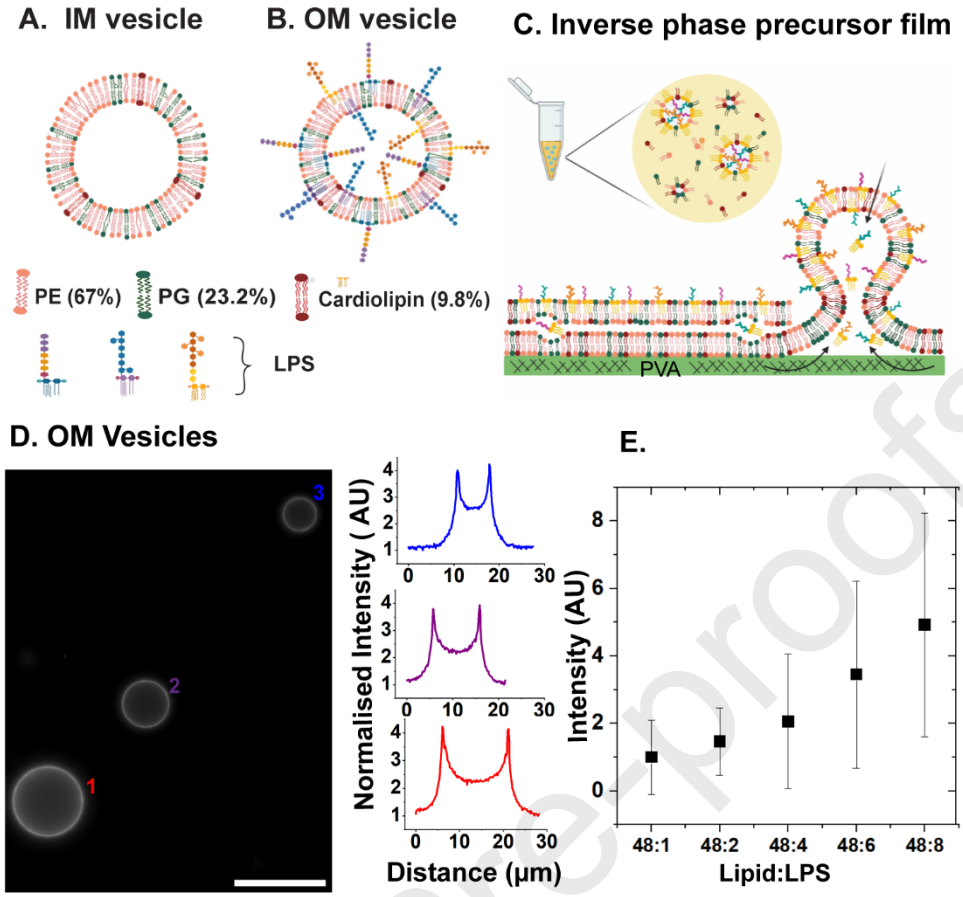

Figure 1. *Native lipid giant vesicle assembly, Schematic of A. IM and B. OM GUVs, C. Inverse phase precursor method for LPS incorporation into the membrane to form vesicles by gel-assisted swelling method, D. LPS incorporated vesicles with Alexa-Fluor 488 LPS (0.25 mol%) in GUVs (unlabelled LPS: IM extract 1:6 initial), Corresponding color-coded rim intensity plot profile shows the peaks of the numbered and color-coded vesicle, E. Plot showing normalized mean rim fluorescence intensities of vesicles (n=60 vesicles for each set,) formed using different IM Lipid: LPS ratio sets. Scale- 20 µm; Conditions- 137mM NaCl, 2.7 mM KCl and 2mM $CaCl_2$ in 10mM HEPES pH 7 is used throughout unless mentioned.*

3.2. Cell-like shape transformation in native lipid-vesicles

3.2.1. IM vesicles membrane transformation

To understand the role of native inner-membrane lipids from bacteria, shape transformation experiments are conducted on IM vesicles without LPS. ATTO-488 (0.5 mol%) or ATTO-550 (0.05 mol%) lipid is incorporated to visualise the transformation in IM vesicles. Two morphologies are mainly observed in osmotically deflated vesicles I. Bud and II. Short nano-tube formation (**Figure 2**A1 to B2). Physical shaping of membranes into bud/tube formation

is depicted (Figure S9 and Video S1). Active membrane fluctuations occur only above $r = 1.6$ and are followed by the appearance of bud/tube (time-resolved statistics *N*=16 batches, *n*=43 independent vesicles). The shape change experiments are conducted with step-wise addition of sucrose (Details in Experimental methods section), where the osmolarity ratio ranged between $1.6 \leq r \leq 1.9$. At $r = 1$ most vesicles are circular and clean (with no structures, 71%), and close to 29% of vesicles have buds on their surface (*N*= 4 batches, *n*= 244 vesicles Table S3). The population of tubulated vesicles increased to 19.6% of vesicles with increasing $r = 1$to $r = 1.9$ as a consequence of the increased area to volume ratio in individual vesicles. The bud population of vesicles is increased to 55 % with increased stress. A small population close to 2.4% is observed for pearl-like/multi-daughter structures (Figure 2C; Figure S10, statistics for $r = 1.9$ from *N*= 7 independent batches, *n*= 204 vesicles). Time-resolved experiments reveal few IM vesicles attempts to transform into multi-daughter morphology but rarely stabilize to form completely closed necks and revert to their original shape, eventually becoming spherical with a bud or tube (Video S1).

For investigating the adsorption of LPS into IM vesicles, we perform shape change experiments of IM vesicles in the presence of the external LPS solution (details in Supporting information text 1.3). External addition of LPS to vesicles did not show any morphologies apart from budding, also observed in IM vesicles. The data reported eliminates the possibility of spontaneous absorption or desorption of LPS in the outer leaflet of IM vesicles under the current experimental conditions (Figure S11, *N*=5 independent batches, *n*= 64 vesicles). We establish that no distinct morphologies are observed in IM vesicles in the presence of external LPS in our system as opposed to simple lipid systems reported [21,22] where asymmetric absorption of glycolipid from solution into outer-leaflet of pre-formed vesicle transformed membranes into curved tubes or pearl-like chains.

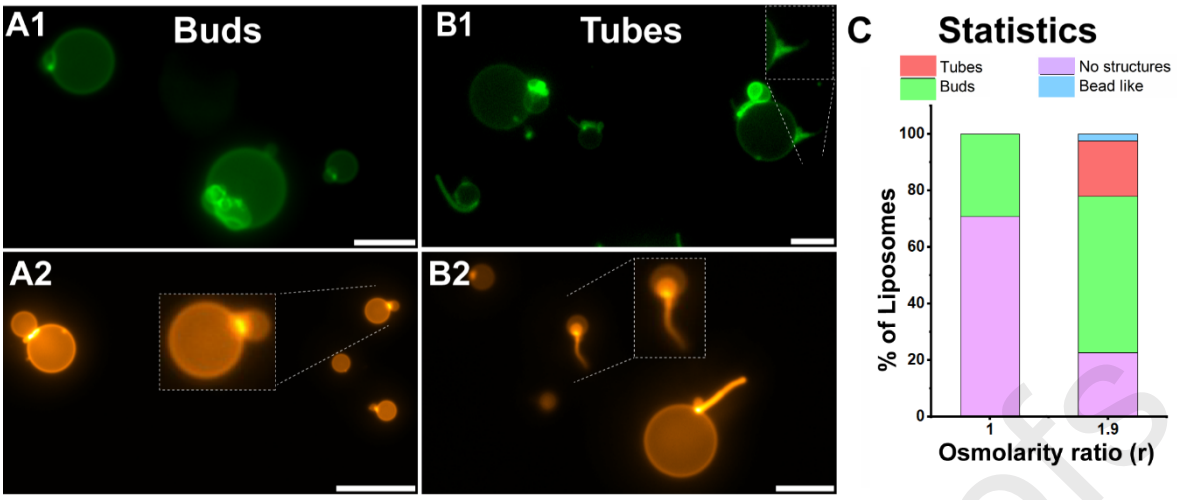

***Figure 2**. Membrane Transformation in vesicles without glycolipids. IM vesicles are labeled with ATTO- 488 DOPE (green color) or ATTO-550 DOPE (orange color), representing lipid displaying A1 and A2. Budding; B1, and B2. Short tubulation morphology in vesicles, Insets show structures or vesicles in zoomed-in form; C. Bar graph showing the percentage of vesicles with different morphologies at an $r = 1$, $r = 1.9$ for both ATTO-488 and ATTO-550 DOPE labeled. Scale bar-10 µm, IM vesicles labeled with 0.5 mol% ATTO 488 or 0.05 mol% ATTO 550 DOPE, false color represents ATTO dye.*

3.2.2. Membrane deformation in OM vesicles

Here, we report the shape changes in OM vesicles with stably reconstituted LPS in them. The osmolarity is increased step-wise to control the volume of a vesicle. Most OM vesicles are circular and lack structures without osmotic pressure (Figure S12). After applying osmotic stress, four different shape transformations are revealed, including (**Figure 3**) I. Budding, II. Nano-tube formation. Transformation initiates by an active membrane fluctuation at $r > 1.2$ in a vesicle, providing a membrane reservoir (Figure 3A, 3B, Video S2). Eventually, a bud or tubulation appears with no further membrane fluctuations of the spherical vesicle (Figure 3A and 3B; Figure S13 A and B). To note, no global deformation intermediate arises when a flaccid OM vesicle forms a bud or nano-tube structure at the corresponding r value. The size of the bud ranges from 600 nm to 3 µm (Table S4). The percentage of bud morphologies is increased from 15% to 27% at $r = 1.3 - 1.4$, where many of the clean circular vesicles form buds. As a result of bud morphologies further transforming into highly curved membranes with increased deflation, the percentage decreases to 4% at higher $r = 1.5 - 1.8$ (Table S3). Nano-tube structures population increases from 3.2% (at $r = 1$) to 9% - 12% of the population at $r = 1.3 - 1.8$, and remain constant throughout the increased deflation.

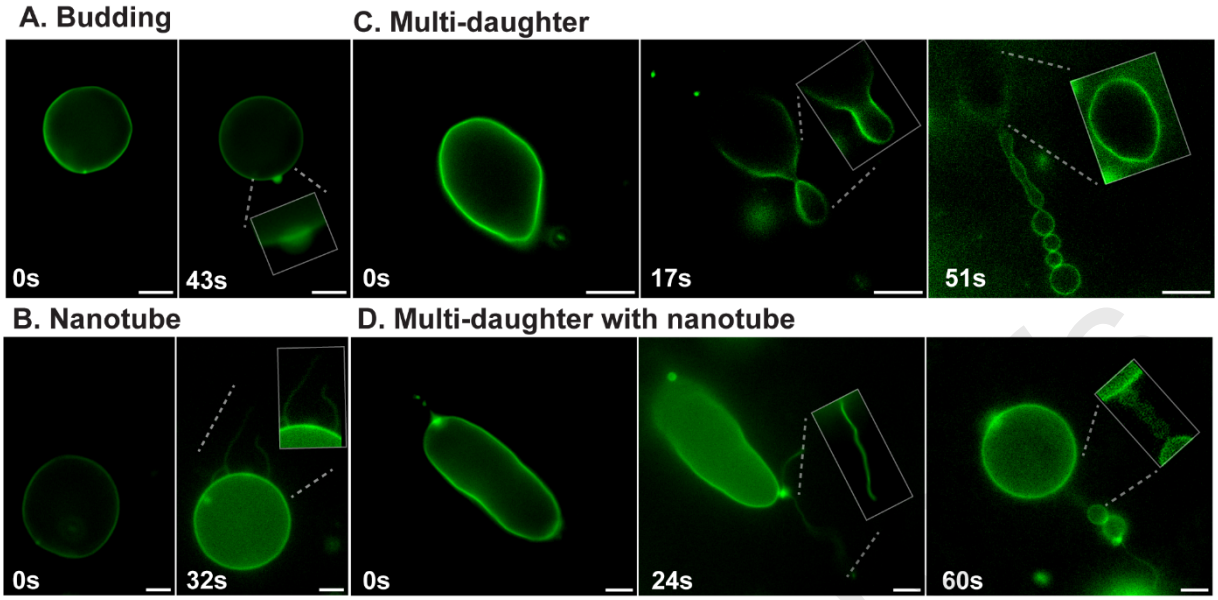

Figure 3. *Real-time membrane remodeling in glycolipid vesicles –Snaps from time-series for a vesicle displaying A. Budding (r = 1.6) where at 0s vesicle is flaccid with membrane fluctuation and 43s the bud is formed, B. Nanotube formation (r = 1.6), 0s the vesicle is flaccid and 32s short nano-tubes are formed, C. Multi-daughter morphology (r = 1.4) at 0s vesicle has changed shape, constriction occurs at 17s, inset shows the transformation just before constriction, at 51s mother vesicle in inset splits into multiple-daughter vesicles, D. Multi-daughter with nano-tube formation (r = 1.5), prolate shaped vesicle at 0s elongates with nano-tube in the inset at 24s, at 60s vesicle is at final morphology with daughter vesicles connected by necks and nano-tubes. Corresponding live changes for each morphology are shown in Video, Video S1 (Bud and nano-tube), Video S2 (Multi-daughter), Video S3 (Multi-daughter with nano-tube). Scale bar: 10 μm for A and C panels, B and D panels are 5 μm, Conditions- FITC-LPS:IM lipid extract (1:6 initial) with 0.5 mol% ATTO-488 DOPE, false color represents ATTO dye, 0s in all structures represent a relative time and not the actual time of addition of hypertonic solutions.*

The other two significant transformations in OM vesicles involve global membrane deformations to form structures, including III. Daughter vesicles connected by necks (Multi-daughter morphology) and IV. Daughter vesicles connected by necks and nano-tubes (Multi-daughter vesicle morphology with nano-tube) (Figure 3C and 3D, Video S3, S4). Such membrane reshaping arises with active membrane fluctuations accompanied by global shape change of vesicle to prolate, elongated, or pear-shaped. Cell-like constriction follows shape

change in vesicles to form dumb-bell structures, preceded by splitting into spherical smaller-sized single/multiple daughter vesicles connected by necks or nano-tubes (Figure 3C, 3D Video S3, S4, S5, Figure S13C, 13D).

Remarkably, the population of multi-daughter vesicles without and with nano-tube structures is regulated with increasing step-wise osmotic stress (from $r = 1.3\ to\ 1.8$), going from 27% to 51% for without nano-tube and 20.6% to 34.3% for with nano-tube structures respectively. The statistical analysis of morphologies is presented (Figure 4C and Table S3) ($r = 1$, calculated from N=9 independent batches, n=156 vesicles; $r = 1.3 - 1.4$ from n=189 vesicles N= 11 batches, $r = 1.5 - 1.8$ from n=384 vesicles, N=13 batches). Furthermore, hydrodynamic flow control experiments reveal that most vesicles are not defective under a flow in the absence of any osmotic stress (Supporting information text 1.3, Figure S14).

Although a time-dependence of sucrose addition for shape transformation in vesicles is performed, we observed that each vesicle transformed to Multi-daughter with or without nano-tubes at different times depending on its initial shape (ranging from a few seconds to tens of minutes). Indeed, we observed that at lower osmotic stress (1.3 – 1.4), 30% of the population of vesicles transform in several minutes into multi-daughter vesicles. However, the remaining population does not stabilize into multi-daughter with or without nano-tube even up to several hours. For bud and nano-tube transformations, the process is relatively faster where most of the vesicles form these structures within minutes. In all of these transformations, the time for structure formation varied largely from vesicle to vesicle. We observed from the time-dependent analysis that the process of transformation and stabilization into highly-curved structures is accelerated in the presence of higher osmotic stress (>1.5); hence universal kinetics of transformation could not be deduced.

Most importantly, stable multi-daughter morphologies are observed here, which seldom revert to their original shape compared to previous studies [21,22]. The IM vesicle morphology data validates that cell-like multi vesicle-nanotube transformations observed in OM vesicles are stabilized by the lipopolysaccharide stably reconstituted in them. LPS is very important in forming and stabilizing the multi-daughter with and without nano-tube structures. Such structures are not formed even in the same or higher osmotic stress generated by sucrose in IM vesicles. In the sections below, we quantitatively determine the elastic parameters of the OM and IM vesicles giving rise to different membrane transformations.

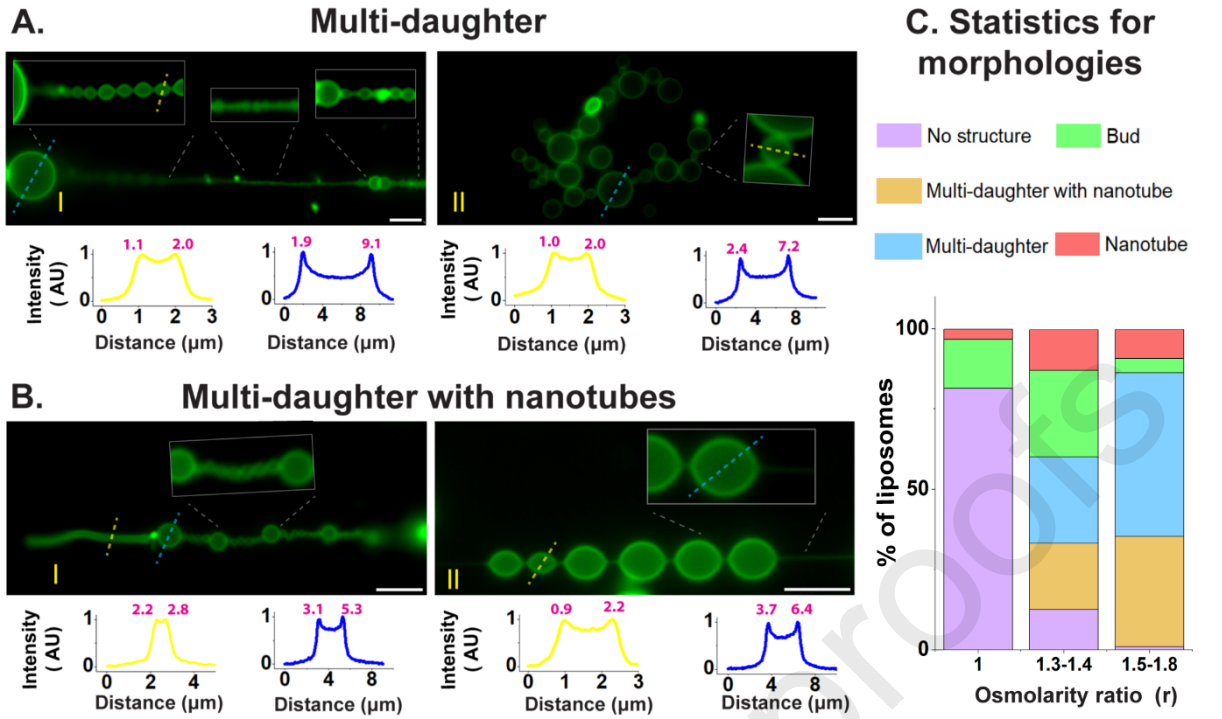

Figure 4. *A multitude of regulated Multi-daughter morphologies A. Only Multi-daughter conformation, B. Multi-daughter structure with nano-tube, I and II indicate two independent morphologies. Insets in both morphologies display out-of-focus structures or zoomed-in images. Corresponding rim intensity profiles for each structure indicate the largest (mother, blue) and smallest resolvable daughter vesicle/nano-tubes (yellow) diameter/thickness based on profiles marked by color-coded arrows in corresponding images. Complete morphology displaying length scales of A I and B II are provided in Figure S16. Scale bar: 5 μm, 0.5 mol% ATTO-488 DOPE represents green false color. C. Bar graph showing the statistics of membrane transformations observed in LPS-vesicles tuned by osmolarity stress defined by r =1, r = 1.3-1.4, and r = 1.5- 1.8. Identical morphologies are observed irrespective of the dye used to label lipid or LPS. The statistics presented are for the following labeling combinations ATTO-488 DOPE labeling the lipid with FITC-LPS, ATTO-488 DOPE, or ATTO-550 DOPE with Alexa-Fluor 488 labeled (0.25 mol%) LPS.*

3.3. Membrane Elastic parameters

We suggest that intrinsic membrane parameters, the spontaneous curvature (m), and bending rigidity (k) from the application of asymmetric sugar solution play a significant role in shaping the IM and OM vesicles [39] (details in Theoretical analysis of morphologies).

3.3.1. Spontaneous Curvature Estimation

We experimentally estimate the spontaneous curvature based on the mean neck curvature values from individual morphologies (eq. 2, 3, and 4). In the case of IM vesicles, we suggest that the spontaneous curvature is generated by sugar asymmetry. As the bud structures form the maximum population of the morphologies observed in IM vesicles, we derived the neck curvatures by calculating the radius of the bud and the vesicle (statistics from n = 50 individual morphologies). The neck curvature of IM vesicles is 0.57± 0.02 μm^{-1}. On the other hand, short nano-tube morphologies form less than 20% of the population (at $r = 1.9$), where the tube diameter is below the resolution limit of the optical set-up (500 nm to 600 nm). The spontaneous curvature of IM vesicles is calculated from the bud geometries by applying the boundary condition that the bud morphology connected to the mother is stable only if the neck connecting the two are stable, i.e., $m \geq M_n$. The lower bound of spontaneous curvature is estimated to be 0.57± 0.02 μm^{-1}.

In the case of OM vesicles, diverse stabilized multi-daughter structures with and without nano-tubes are reported. The daughter vesicle's size varied stochastically in the range of one order of magnitude in the same morphology (**Figure 4, Figure 5,** and Figure S15). Thus, an OM vesicle multi-daughter morphology can harbor diverse curvatures, comprising mainly optically resolved daughter vesicles (600 nm ≤ d≤ 6 µm) (Figure 4A II), unresolved pearl-like structures (d < 600 nm) (Figure S15 AI), or both in the same stable morphological state (Figure 4AI, Figure S15 A III, and Figure S16). Hence, the estimation of neck curvature of such membranes is theoretically complex due to the diverse range of morphologies attained. However, we estimate spontaneous curvature based on the geometry of the morphologies.

The multi-daughter morphologies are stable due to the stable membrane necks connecting adjacent daughter vesicles and hence would have to satisfy the boundary condition of spontaneous curvature $m \geq M_n$. Notably, we calculate using eq. 3 the highest neck curvature by measuring the two smallest adjacent daughter vesicles of the individual multi-daughter structures as it forms one of the largest populations of morphologies (at $r = 1.5 - 1.8$). Based on the geometry of the optically resolved daughter vesicles, the average neck curvature is estimated to be 1.74 ± 0.1 μm^{-1} (Figure 5B, N = 51 morphologies).

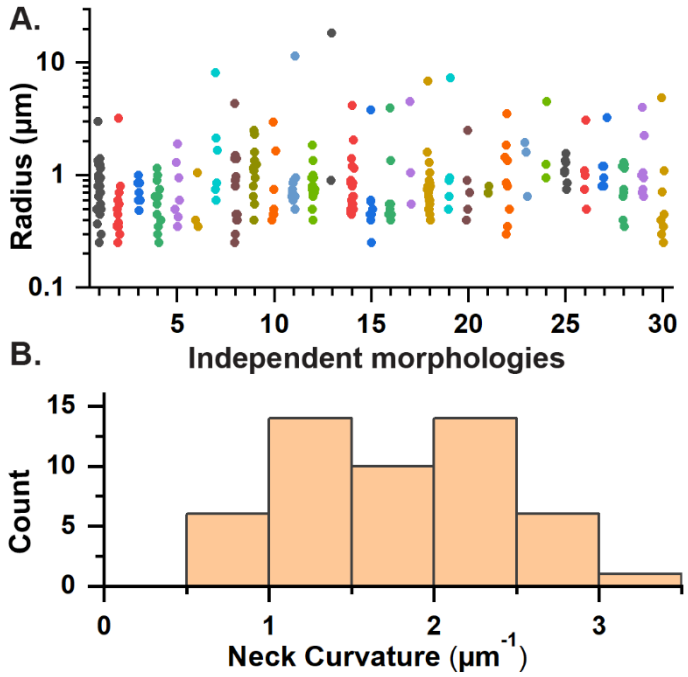

Figure 5*: Statistical analysis of radius and corresponding neck curvatures A. Scatter plot comparing the radius of individual daughter vesicles in a stabilized transformation depicting 30 different morphologies. Each color depicts individual morphology with varied daughter vesicle radius B. Histogram showing membrane neck curvature of morphologies estimated from the smallest (resolvable) connecting daughter vesicles in individual morphologies.*

As the nano-tubes are all observed outside the vesicle, the sign convention of curvature is positive. Multi-daughter structures connected by nano-tubes in OM vesicles (Figure 4B, Figure 4B) can attain a highly dynamic tube structure directly attached to the mother vesicle (Figure 4B I, Figure S15B I, Video S6). Stable long-range (up to 200 μm length) membrane tube networks connecting daughter vesicles are observed (Figure 4B II, Figure S15B II). We estimate the spontaneous curvature (lower bound) to be 1.74 ± 0.1 μm^{-1} from the neck curvature of the optically resolved multi-daughter morphologies. Further, we calculate the spontaneous curvature (upper bound) of OM vesicles using eq. 4 and obtain a range of 3-10 μm^{-1} based on the estimated geometry of the nano-tube structures (radius approx. 50-150 nm SI 1.4).

The experimentally calculated neck curvature for IM vesicles is accurate as most of the morphologies observed in IM are optically resolved, unlike in OM vesicles. However, the neck curvature of OM vesicles is an underestimation primarily limited by optical resolution. Importantly, we can conclude that even the lower bound spontaneous curvature of OM vesicles is more significant than IM vesicles under identical aqueous environments or sugar asymmetries. Previously, small (2 to 4 mol%) glycolipid asymmetries generated large spontaneous curvatures

and formed curved membrane structures [10,19,21]. We can suggest that apart from asymmetric exposure to sugar solutions, even slight asymmetric reconstitution of LPS can generate a sizeable spontaneous curvature that allows OM vesicles to deform globally into highly curved structures instead of IM vesicles.

3.3.2. Bending Rigidity

We determined the bending modulus of the IM and OM vesicles to investigate their role in deformation using non-confocal "flickering" experiments [35,36,40]. Bending modulus is calculated from undulations of vesicles, where a visible difference in the fluctuations is observed in IM compared to OM vesicles (Video S7). Only 2% of IM vesicles show visible fluctuations, whereas 95% of OM vesicles fluctuate before transforming. **Figure 6** shows the typical dependence of the variance of the spectrum amplitude with the optical mode for IM (Figure 6A) and OM vesicles (Figure 6B). Overall, IM vesicles are stiffer than OM vesicles as reflected by larger bending rigidity values κ_{IM} ~37.5 ± 11.2 k_BT for IM vesicles (n=3 vesicles, Figure 6C, Table S2), which is higher than the κ_{POPC} ~ 25 k_BT, as expected for charged species [41]. OM vesicles exhibit lower bending rigidity than IM vesicles (Figure 6B) with an average value of κ_{OM}~15 ± 11.5 k_BT (n=11 vesicles), consistent with previous literature on the effect of the addition of glycolipids in the bending rigidity of the vesicle [16,19]. The fitted values for the bending rigidity of OM vesicles (Figure S17, Table S2) vary more than for IM vesicles, probably due to the variability in LPS reconstitution from vesicle to vesicle.

Interestingly, OM vesicles and IM vesicles cluster in different regions in the transmembrane tension versus bending rigidity map depicting significantly different mechanical properties of the two membranes (Figure 6C). As shown in Figure 6C, the membrane tension of the OM vesicles is higher than that of IM vesicles, as σ is proportional to the local curvature of the membrane [36]. Therefore, the observed OM vesicles have lower bending rigidity and higher membrane tension than the IM vesicles.

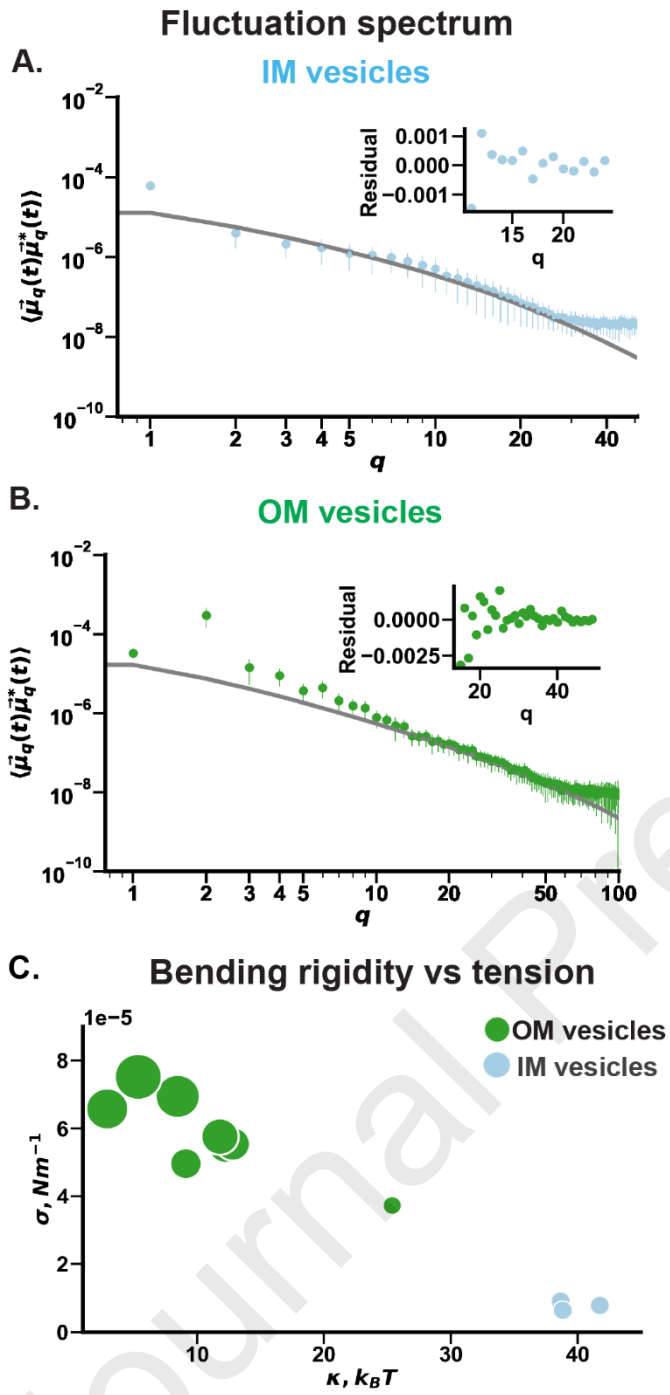

***Figure 6**: Bending rigidity and membrane tension extrapolation. Fluctuation spectrum with the best fit to the variance of the amplitude, $<\overrightarrow{\mu_q(t)}\overrightarrow{\mu_q^*(t)}>$, dependence on the mode number. Fit residuals are shown as inset for the optical modes used for the fit for an individual. A. IM vesicles. B. LPS vesicle. C. Fitted bending rigidity versus membrane tension (experimentally extracted $H_o^{IM} = 0.57\ \mu m^{-1}$, $H_o^{OM} = 3\mu m^{-1}$) for all the vesicles analyzed, Table S2. The filled circles in C represent individual vesicles, and the circle size represents the size of the vesicle.*

We can conclude that LPS incorporated into the vesicles drastically changes the bending rigidity (k), making the OM membranes softer that helps transform the membrane into curved structures. We emphasize that the data reported here provide a quantitative description of membrane deformation under physiologically relevant conditions that closely mimic the bacterial membrane. Further, our findings may help elucidate mechanistic descriptions of structures like nano-tubes and outer membrane vesicles observed in cells.

Glycolipids and proteins from eukaryotic systems have previously demonstrated curved membrane structures via crowding or steric pressure mechanism [20,42,43]. In most of these systems, the glycocalyx or native lipids are asymmetrically constituted in the outer leaflets of the cell membrane or vesicle membranes, generating steric pressure with increasing polymer density [20]. As the vesicle systems generated in this study are not entirely asymmetric, such a polymer-brush mechanism may not be a primary reason for the bending of membranes; however, it cannot be completely ruled out. We affirm that the large spontaneous curvature generated by a slight asymmetry and lower bending rigidity in OM vesicles compared to IM vesicles is the foremost cause for large-scale bending in OM vesicles.

Previously, Min protein-assisted deformation via curvature generation mechanism in vesicles mimicking IM(without LPS) displayed similar morphologies, including budding, tubulation, and occasionally large-scale deformation into dumb-bell structures and splitting into daughter vesicles [7,8]. Remarkably, the OM vesicle system demonstrated in our study provides diverse topologies mimicking bacterial cell morphologies and their length scales [44,45], including nano-wires connecting cells and nano-tube communication networks, in a protein-free environment. As no control over the structures of morphology is attained in the current experimental conditions in OM vesicles, we assert curvature generating bacterial proteins may be required for control over the deformation process or complete fission of such morphologies [46].

4. Conclusion

Lipopolysaccharide is stably reconstituted in a physiologically relevant bacterial lipid vesicle (OM) system using a simple single-step gel-assisted lipid hydration for deformation investigations. Global shape transformations triggered exclusively in OM vesicles demonstrate highly-curved stable topologies with diverse curvatures, mimicking cell structures absent in IM vesicles with no LPS. We quantify the role of LPS assembly in vesicles forming curved

structures in terms of their membrane mechanical properties. Firstly, mild asymmetric LPS assembly generates a large spontaneous curvature in OM vesicles (lower bound: 1.74 ± 0.1 μm^{-1}, upper bound: 3-10 μm^{-1}) as compared to IM vesicles (0.57 ± 0.02 μm^{-1}). Finally, LPS in vesicles lowers their bending rigidity (15 ± 11.5 k_BT) compared to IM vesicles (37.5 ± 11.2 k_BT). We conclude that a higher spontaneous curvature and lower bending rigidity play a significant role in the global transformation of the OM vesicles. We present a quantitative analysis of native lipid's role in membrane bending with implications in cell-membrane remodeling, which remained obscure due to the technical challenges of stable glycolipid assembly [21,22]. We suggest the engineered vesicles demonstrated here will help understand membrane-interface processes like curvature sensing or pore formation mechanism by membrane proteins and antimicrobial peptides in a native lipid environment.

Supporting Information

Supporting information is available free of charge.

Author Contributions

Karthika S Nair: Investigation, Validation, Formal Analysis, Writing - Review & Editing, Visualization, **Neethu B Raj**: Investigation, Validation, Formal Analysis **K Madhavan Nampoothiri**: Investigation, Writing - Review & Editing, **Gayathri Mohanan**: Investigation, **Silvia Acosta-Gutiérrez:** Formal Analysis, Supervision, Writing – Review & Editing, **Harsha Bajaj**: Conceptualization, Formal analysis, Visualization, Writing - Original Draft, Supervision, Funding acquisition.

Acknowledgments

The work is supported by the 'Innovative Young Biotechnologist Award' and 'Biotechnology Career Advancement and Reorientation Programme' by the Department of Biotechnology, Government of India (BT/11/IYBA/2018/09; BT/PR18365/BIC/101/487/2016). HB acknowledges Dr. A. Ajayaghosh**,** the Director CSIR-NIIST, for support for the lab facilities. HB thanks Dr. Rajeev K Sukumaran, Dr. Ramesh Kumar N, and Dr. Raghu K G for the equipment support. SAG and HB thank Dr. Davide Orsi and Dr. Pietro Cicuta for their helpful discussions on bending rigidity calculations. HB thanks Dr. Jehangir Cama, Dr. Jan Steinkühler, and Dr. Ahanjit Bhattacharya for their helpful discussions.

References

[1] J.G. Carlton, H. Jones, U.S. Eggert, Membrane and organelle dynamics during cell division, Nat. Rev. Mol. Cell Biol. 21 (2020) 151–166. https://doi.org/10.1038/s41580-019-0208-1.

[2] W. Kukulski, M. Schorb, M. Kaksonen, J.A.G. Briggs, Plasma membrane reshaping during endocytosis is revealed by time-resolved electron tomography, Cell. 150 (2012) 508–520. https://doi.org/10.1016/j.cell.2012.05.046.

[3] S. Pande, S. Shitut, L. Freund, M. Westermann, F. Bertels, C. Colesie, I.B. Bischofs, C. Kost, Metabolic cross-feeding via intercellular nano-tubes among bacteria, Nat. Commun. 6 (2015) 1–13. https://doi.org/10.1038/ncomms7238.

[4] D.M. Davis, S. Sowinski, Membrane nano-tubes: Dynamic long-distance connections between animal cells, Nat. Rev. Mol. Cell Biol. 9 (2008) 431–436. https://doi.org/10.1038/nrm2399.

[5] T. Harayama, H. Riezman, Understanding the diversity of membrane lipid composition, Nat. Rev. Mol. Cell Biol. 19 (2018) 281–296. https://doi.org/10.1038/nrm.2017.138.

[6] R. Dimova, Giant Vesicles and Their Use in Assays for Assessing Membrane Phase State, Curvature, Mechanics, and Electrical Properties, Annu. Rev. Biophys. 48 (2019) 93–119. https://doi.org/10.1146/annurev-biophys-052118-115342%0A%0A.

[7] E. Godino, JN López, D. Foschepoth, C. Cleij, A. Doerr, C.F. Castellà, C. Danelon, De novo synthesized Min proteins drive oscillatory liposome deformation and regulate FtsA-FtsZ cytoskeletal patterns, Nat. Commun. 10 (2019) 1–12. https://doi.org/10.1038/s41467-019-12932-w.

[8] T. Litschel, B. Ramm, R. Maas, M. Heymann, P. Schwille, Beating Vesicles: Encapsulated Protein Oscillations Cause Dynamic Membrane Deformations, Angew. Chemie Int. Ed. 57 (2018) 16286–16290. http://doi.wiley.com/10.1002/anie.201808750.

[9] K.A. Ganzinger, A. Merino-Salomón, D.A. García-Soriano, A.N. Butterfield, T. Litschel, F. Siedler, P. Schwille, FtsZ Reorganization Facilitates Deformation of Giant Vesicles in Microfluidic Traps, Angew. Chemie. 132 (2020) 21556–21560. https://doi.org/10.1002/ange.202001928.

[10] T. Bhatia, J. Agudo-Canalejo, R. Dimova, R. Lipowsky, Membrane Nanotubes Increase the Robustness of Giant Vesicles, ACS Nano. 12 (2018) 4478–4485.

https://doi.org/10.1021/acsnano.8b00640.

[11] D. Garenne, A. Libchaber, V. Noireaux, Membrane molecular crowding enhances MreB polymerization to shape synthetic cells from spheres to rods, Proc. Natl. Acad. Sci. U. S. A. 117 (2020) 1902–1909. https://doi.org/10.1073/pnas.1914656117.

[12] J. Steinkühler, R.L. Knorr, Z. Zhao, T. Bhatia, S.M. Bartelt, S. Wegner, R. Dimova, R. Lipowsky, Controlled division of cell-sized vesicles by low densities of membrane-bound proteins, Nat. Commun. 11 (2020) 1–11. https://doi.org/10.1038/s41467-020-14696-0.

[13] T. Bhatia, S. Christ, J. Steinkühler, R. Dimova, R. Lipowsky, Simple sugars shape giant vesicles into multispheres with many membrane necks, Soft Matter. 16 (2020) 1246–1258. https://doi.org/10.1039/C9SM01890E%0A.

[14] C. Schwechheimer, M.J. Kuehn, Outer-membrane vesicles from Gram-negative bacteria: biogenesis and functions, Nat. Rev. Microbiol. 13 (2015) 605–619. https://doi.org/10.1038/nrmicro3525%0A%0A.

[15] J.C.M. Holthuis, A.K. Menon, Lipid landscapes and pipelines in membrane homeostasis, Nature. 510 (2014) 48–57. https://doi.org/10.1038/nature13474.

[16] N. Fricke, R. Dimova, GM1 Softens POPC Membranes and Induces the Formation of Micron-Sized Domains, Biophys. J. 111 (2016) 1935–1945. https://doi.org/10.1016/j.bpj.2016.09.028.

[17] B. Come, M. Donato, L.F. Potenza, P. Mariani, R. Itri, F. Spinozzi, The intriguing role of rhamnolipids on plasma membrane remodelling: From lipid rafts to membrane budding, J. Colloid Interface Sci. 582 (2021) 669–677. https://doi.org/10.1016/j.jcis.2020.08.027.

[18] H. Ewers, W. Römer, A.E. Smith, K. Bacia, S. Dmitrieff, W. Chai, R. Mancini, J. Kartenbeck, V. Chambon, L. Berland, A. Oppenheim, G. Schwarzmann, T. Feizi, P. Schwille, P. Sens, A. Helenius, L. Johannes, GM1 structure determines SV40-induced membrane invagination and infection, Nat. Cell Biol. 12 (2010) 11–18. https://doi.org/10.1038/ncb1999%0A%0A.

[19] R. Dasgupta, MS Miettinen, N. Fricke, R. Lipowsky, R. Dimova, The glycolipid GM1 reshapes asymmetric biomembranes and giant vesicles by curvature generation, Proc. Natl. Acad. Sci. U. S. A. 115 (2018) 5756–5761. https://doi.org/10.1073/pnas.1722320115.

[20] C.R. Shurer, J.C.H. Kuo, L.D.M. Roberts, J.G. Gandhi, M.J. Colville, T.A. Enoki, H.

Pan, J. Su, J.M. Noble, M.J. Hollander, J.P. O'Donnell, R. Yin, K. Pedram, L. Möckl, L.F. Kourkoutis, W.E. Moerner, C.R. Bertozzi, G.W. Feigenson, H.L. Reesink, M.J. Paszek, Physical Principles of Membrane Shape Regulation by the Glycocalyx, Cell. 177 (2019) 1757-1770.e21. https://doi.org/10.1016/J.CELL.2019.04.017.

[21] J.M. Alam, M. Yamazaki, Spontaneous insertion of lipopolysaccharide into lipid membranes from aqueous solution, Chem. Phys. Lipids. 164 (2011) 166–174. https://doi.org/10.1016/j.chemphyslip.2010.12.008.

[22] M. Mally, B. Božič, S.V. Hartman, U. Klančnik, M. Mur, S. Svetina, J. Derganc, Controlled shaping of lipid vesicles in a microfluidic diffusion chamber, RSC Adv. 7 (2017) 36506–36515. https://doi.org/10.1039/C7RA05584F%0A.

[23] J. Kubiak, J. Brewer, S. Hansen, L.A. Bagatolli, Lipid lateral organization on giant unilamellar vesicles containing lipopolysaccharides., Biophys. J. 100 (2011) 978–986. https://doi.org/10.1016/j.bpj.2011.01.012.

[24] S. Maktabi, J.W. Schertzer, P.R. Chiarot, Dewetting-induced formation and mechanical properties of synthetic bacterial outer membrane models (GUVs) with controlled inner-leaflet lipid composition, Soft Matter. 15 (2019) 3938–3948. https://doi.org/10.1039/C9SM00223E.

[25] A. Weinberger, F.-C. Tsai, G.H. Koenderink, T.F. Schmidt, R. Itri, W. Meier, T. Schmatko, A. Schröder, C. Marques, Gel-assisted formation of giant unilamellar vesicles., Biophys. J. 105 (2013) 154–164. 10.1016/j.bpj.2013.05.024.

[26] G. Mohanan, K.S. Nair, K.M. Nampoothiri, H. Bajaj, Engineering bio-mimicking functional vesicles with multiple compartments for quantifying molecular transport, Chem. Sci. 11 (2020) 4669–4679. https://doi.org/10.1039/D0SC00084A%0A.

[27] M. Schaich, D. Sobota, H. Sleath, J. Cama, U.F. Keyser, Characterization of lipid composition and diffusivity in OLA generated vesicles, Biochim. Biophys. Acta - Biomembr. 1862 (2020) 183359. https://doi.org/10.1016/J.BBAMEM.2020.183359.

[28] L. Paulowski, A. Donoghue, C. Nehls, S. Groth, M. Koistinen, S.O. Hagge, A. Böhling, M. Winterhalter, T. Gutsmann, The Beauty of Asymmetric Membranes: Reconstitution of the Outer Membrane of Gram-Negative Bacteria, Front. Cell Dev. Biol. 8 (2020). https://doi.org/10.3389/fcell.2020.00586.

[29] J. Steinkühler, P. De Tillieux, R.L. Knorr, R. Lipowsky, R. Dimova, Charged giant unilamellar vesicles prepared by electroformation exhibit nano-tubes and transbilayer lipid asymmetry, Sci. Rep. 8 (2018) 11838. https://doi.org/10.1038/s41598-018-30286-

z%0A%0A.

[30] R. Lipowsky, Spontaneous tubulation of membranes and vesicles reveals membrane tension generated by spontaneous curvature, Faraday Discuss. 161 (2012) 305–331. https://doi.org/10.1039/c2fd20105d.

[31] U. Seifert, K. Berndl, R. Lipowsky, Shape transformations of vesicles: Phase diagram for spontaneous- curvature and bilayer-coupling models, Phys. Rev. A. 44 (1991) 1182–1202. https://doi.org/10.1103/PhysRevA.44.1182.

[32] R. Lipowsky, R. Dimova, Introduction to remodeling of biomembranes, Soft Matter. 17 (2021) 214–221. https://doi.org/10.1039/D0SM90234A%0A.

[33] R. Lipowsky, Understanding giant vesicles: A theoretical perspective, in: Giant Vesicle B., CRC Press, 2020: pp. 73–168. https://doi.org/10.1201/9781315152516-5.

[34] Y. Li, R. Lipowsky, R. Dimova, Membrane nano-tubes induced by aqueous phase separation and stabilized by spontaneous curvature, Proc. Natl. Acad. Sci. U. S. A. 108 (2011) 4731–4736. https://doi.org/10.1073/pnas.1015892108.

[35] R.D. Usery, T.A. Enoki, SP Wickramasinghe, V.P. Nguyen, D.G. Ackerman, D. V. Greathouse, R.E. Koeppe, F.N. Barrera, G.W. Feigenson, Membrane Bending Moduli of Coexisting Liquid Phases Containing Transmembrane Peptide, Biophys. J. 114 (2018) 2152–2164. https://doi.org/10.1016/J.BPJ.2018.03.026.

[36] S.A. Rautu, D. Orsi, L. Di Michele, G. Rowlands, P. Cicuta, M.S. Turner, The role of optical projection in the analysis of membrane fluctuations, Soft Matter. 13 (2017) 3480–3483. https://doi.org/10.1039/c7sm00108h.

[37] P. Virtanen, R. Gommers, T.E. Oliphant, M. Haberland, T. Reddy, D. Cournapeau, E. Burovski, P. Peterson, W. Weckesser, J. Bright, S.J. van der Walt, M. Brett, J. Wilson, K.J. Millman, N. Mayorov, A.R.J. Nelson, E. Jones, R. Kern, E. Larson, C.J. Carey, İ. Polat, Y. Feng, E.W. Moore, J. VanderPlas, D. Laxalde, J. Perktold, R. Cimrman, I. Henriksen, E.A. Quintero, C.R. Harris, A.M. Archibald, A.H. Ribeiro, F. Pedregosa, P. van Mulbregt, A. Vijaykumar, A. Pietro Bardelli, A. Rothberg, A. Hilboll, A. Kloeckner, A. Scopatz, A. Lee, A. Rokem, C.N. Woods, C. Fulton, C. Masson, C. Häggström, C. Fitzgerald, D.A. Nicholson, D.R. Hagen, D. V. Pasechnik, E. Olivetti, E. Martin, E. Wieser, F. Silva, F. Lenders, F. Wilhelm, G. Young, G.A. Price, G.L. Ingold, G.E. Allen, G.R. Lee, H. Audren, I. Probst, J.P. Dietrich, J. Silterra, J.T. Webber, J. Slavič, J. Nothman, J. Buchner, J. Kulick, J.L. Schönberger, J.V. de Miranda Cardoso, J. Reimer, J. Harrington, J.L.C. Rodríguez, J. Nunez-Iglesias, J.

Kuczynski, K. Tritz, M. Thoma, M. Newville, M. Kümmerer, M. Bolingbroke, M. Tartre, M. Pak, N.J. Smith, N. Nowaczyk, N. Shebanov, O. Pavlyk, P.A. Brodtkorb, P. Lee, R.T. McGibbon, R. Feldbauer, S. Lewis, S. Tygier, S. Sievert, S. Vigna, S. Peterson, S. More, T. Pudlik, T. Oshima, T.J. Pingel, T.P. Robitaille, T. Spura, T.R. Jones, T. Cera, T. Leslie, T. Zito, T. Krauss, U. Upadhyay, Y.O. Halchenko, Y. Vázquez-Baeza, SciPy 1.0: fundamental algorithms for scientific computing in Python, Nat. Methods 2020 173. 17 (2020) 261–272. https://doi.org/10.1038/s41592-019-0686-2.

[38] P.F. Muhlradt, J. Menzel, J.R. Golecki, V. Speth, Lateral Mobility and Surface Density of Lipopolysaccharide in the Outer Membrane of Salmonella typhimurium, Eur. J. Biochem. 43 (1974) 533–539. http://doi.wiley.com/10.1111/j.1432-1033.1974.tb03440.x.

[39] R. Lipowsky, Understanding and controlling the morphological complexity of biomembranes, Adv. Biomembr. Lipid Self-Assembly. 30 (2019) 105–157. https://doi.org/10.1016/bs.abl.2019.10.002.

[40] C. Esposito, A. Tian, S. Melamed, C. Johnson, S.Y. Tee, T. Baumgart, Flicker spectroscopy of thermal lipid bilayer domain boundary fluctuations, Biophys. J. 93 (2007) 3169–3181. https://doi.org/10.1529/biophysj.107.111922.

[41] H.A. Faizi, S.L. Frey, J. Steinkühler, R. Dimova, P.M. Vlahovska, Bending rigidity of charged lipid bilayer membranes, Soft Matter. 15 (2019) 6006–6013. https://doi.org/10.1039/c9sm00772e.

[42] J.C. Stachowiak, E.M. Schmid, C.J. Ryan, H.S. Ann, D.Y. Sasaki, M.B. Sherman, P.L. Geissler, D.A. Fletcher, C.C. Hayden, Membrane bending by protein-protein crowding, Nat. Cell Biol. 14 (2012) 944–949. https://www.nature.com/articles/ncb2561 (accessed November 4, 2020).

[43] D.J. Busch, J.R. Houser, C.C. Hayden, M.B. Sherman, E.M. Lafer, J.C. Stachowiak, Intrinsically disordered proteins drive membrane curvature, Nat. Commun. 2015 61. 6 (2015) 1–11. https://doi.org/10.1038/ncomms8875.

[44] P. Subramanian, S. Pirbadian, M.Y. El-Naggar, G.J. Jensen, Ultrastructure of Shewanella oneidensis MR-1 nano-wires revealed by electron cryotomography, Proc. Natl. Acad. Sci. U. S. A. 115 (2018) E3246–E3255. https://doi.org/10.1073/pnas.1718810115.

[45] C. Schwechheimer, M.J. Kuehn, Outer-membrane vesicles from Gram-negative

bacteria: biogenesis and functions., Nat. Rev. Microbiol. 13 (2015) 605–19. https://doi.org/10.1038/nrmicro3525%0A%0A.

[46] M. Osawa, H.P. Erickson, Liposome division by a simple bacterial division machinery, Proc. Natl. Acad. Sci. U. S. A. 110 (2013) 11000–11004. https://doi.org/10.1073/pnas.1222254110.

Karthika S Nair: Investigation, Validation, Formal Analysis, Writing - Review & Editing, Visualization, **Neethu B Raj**: Investigation, Validation, Formal Analysis **K Madhavan Nampoothiri**: Investigation, Writing - Review & Editing, **Gayathri Mohanan**: Investigation, **Silvia Acosta-Gutiérrez:** Formal Analysis, Supervision, Writing – Review & Editing, **Harsha Bajaj**: Conceptualization, Formal analysis, Visualization, Writing - Original Draft, Supervision, Funding acquisition.

Declaration of interests

☒ The authors declare that they have no known competing financial interests or personal relationships that could have appeared to influence the work reported in this paper.

☐The authors declare the following financial interests/personal relationships which may be considered as potential competing interests: